

# Seven energy/temperature scales in hole-doped cuprates

A Mourachkine

Free University of Brussels, CP-232, Blvd du Triomphe, B-1050 Brussels, Belgium

(Received)

**Abstract** The purpose of this paper is to discuss a phase diagram of hole-doped cuprates. Hole-doped cuprates have a very rich phase diagram as a function of doping. This is due to a charge inhomogeneity in  $\text{CuO}_2$  planes: the charge distribution in  $\text{CuO}_2$  planes is inhomogeneous both on a nanoscale and macroscale. Depending on the doping level, the  $\text{CuO}_2$  planes comprise at least four different types of clusters having a size of a few nanometers. Each type of clusters has its own features. As a consequence, the common phase diagram consists of, at least, seven different energy/temperature scales. As an example, we consider a phase diagram of  $\text{Bi}_2\text{Sr}_2\text{CaCu}_2\text{O}_{8+x}$ .

## I. INTRODUCTION

The phenomenon of high- $T_c$  superconductivity was discovered in cuprates [1]. The understanding of a phase diagram of cuprates is important since it is directly related to the understanding of the physics of high- $T_c$  superconductors.

In the literature, one can find a few different phase diagrams for superconducting cuprates. As an example, figure 1 shows four different phase diagrams of hole-doped cuprates, taken from the literature. All four phase diagrams show the commensurate antiferromagnetic phase at low doping level  $p$  and the superconducting phase with a transition temperature  $T_c$ . These two phases are long-ranged. The commensurate antiferromagnetic phase appears at a Néel temperature  $T_N$ . If in  $\text{La}_{2-x}\text{Sr}_x\text{CuO}_4$  (LSCO), these two phases are separated by some distance, in  $\text{YBa}_2\text{Cu}_3\text{O}_{6+x}$  (YBCO) the distance between them is almost absent. In spite of this and some other small differences, there is good agreement on the existence of these two phases in the phase diagram of superconducting cuprates. In figure 1, one can see that the disagreement among all these phase diagrams is mainly in the dispositions of the temperature scales situated above the superconducting phase. In other words, there is no consensus on the physics of normal state of cuprates.

Soon after the discovery of high- $T_c$  superconductivity it became clear that the understanding of normal-state properties of cuprates is crucial for the understanding of the mechanism of high- $T_c$  superconductivity. Indeed, there is an interesting contrast between the development of the physics of cuprates and that of the physics of conventional superconductors. Just before the creation of the BCS theory, the normal-state properties of conventional metals were very well understood; however superconductivity was not. The situation with the cuprates was just the opposite: at the time high- $T_c$  superconductivity was discovered, there already existed a good understanding of the phenomenon of superconductivity, but the normal-state properties of the cuprates were practically unknown. What is interesting is that 16 years after

the discovery [1] their normal-state properties are still “unknown.” The problem is not that there is no explanation of these unusual properties, the problem is that there are too many of them.

There is good agreement on the existence of the so-called pseudogap which occur at  $T^* > T_c$ . There is *even* consensus on the doping dependence of pseudogap in hole-doped cuprates: the magnitude of pseudogap decreases as the doping level increases. However, here the common agreement ends. Further there is a polarization of opinions based either on different measurements or on different theories. First, there is no yet consensus on the presence of preformed Cooper pairs above  $T_c$  in cuprates. Secondly, there is no agreement on the exact doping dependence of temperature (energy) scale  $T^*$ .

The question concerning the presence of preformed Cooper pairs above  $T_c$  in cuprates is not the main topic of this paper, therefore we are not going to discuss it here. There are enough evidence in the literature for the presence of preformed Cooper pairs above  $T_c$  in cuprates (see references in [2] and [3]). The purpose of this paper is to discuss the second issue raised above, namely, the doping dependences of different temperature/energy scales in hole-doped cuprates and their origins. Hole-doped cuprates have a very rich phase diagram as a function of doping. This is due to a charge inhomogeneity in  $\text{CuO}_2$  planes: the charge distribution in  $\text{CuO}_2$  planes is inhomogeneous both on a nanoscale and macroscale. Depending on the doping level, the  $\text{CuO}_2$  planes comprise at least four different types of clusters having a size of a few nanometers. Each type of clusters has its own features. As a consequence, the common phase diagram consists of, at least, seven different energy/temperature scales. As an example, we consider a phase diagram of  $\text{Bi}_2\text{Sr}_2\text{CaCu}_2\text{O}_{8+x}$  (Bi2212).

## II. DIFFERENT PHASE DIAGRAMS

In figure 1, the first two phase diagrams are based on experimental data: the phase diagram shown in figure

1(a) is mainly inferred from nuclear magnetic resonance, specific heat and resistivity measurements (see references in [3]). The phase diagram in figure 1(b) is based on tunneling and angle-resolved photoemission (ARPES) measurements. In figure 1(b), the pseudogap temperature scale  $T^*$  is inferred from bias positions of humps in tunneling and ARPES spectra, while the positions of main peaks in these spectra determine the pairing temperature/energy scale  $T_0$  corresponding to the formation of incoherent Cooper pairs. The phase diagrams in figures 1(c) and 1(d) are purely theoretical and based on the idea of the existence of two types of superconductivity: an unconventional type in underdoped cuprates and a BCS type in overdoped cuprates. They emerge near the optimally doped region of superconducting phase.

Leaving the phase diagrams shown in figures 1(c) and 1(d) for further theoretical considerations, we focus our attention exclusively on experimental data presented in figures 1(a) and 1(b). The question is why do different experimental techniques give different energy/temperature scales? This question is directly related to the understanding of normal-state properties of cuprates.

### III. PHASE DIAGRAM OF BI2212

Figure 2 shows an idealized phase diagram of Bi2212 taken from [3], in which the spin-glass temperature scale  $T_g$  is added. This temperature/energy scale was recently observed in Bi2212 by muon spin relaxation measurements [4]. Figure 2 shows six different temperature/energy scales in Bi2212. The seventh temperature scale—the commensurate antiferromagnetic phase at low doping level—is not shown because it was not yet observed in Bi2212: There is a technical problem to synthesize large-size good-quality *undoped* single crystals of Bi2212, which are necessary for neutron scattering measurements. In fact, the commensurate antiferromagnetic phase is not the primary focus of this paper. It is worth noting that the phase diagram of Bi2212 in figure 2 is **not** universal but reflects main features of the physics involved in all cuprates. First, the temperature scales in figure 2 will be given explicitly, and then we discuss their origins.

The superconducting phase appears at a critical temperature  $T_c$  shown in figure 2. In Bi2212, the doping dependence  $T_c(p)$  can be expressed [5] as

$$T_c(p) \simeq T_{c,max}[1 - 82.6(p - 0.16)^2]. \quad (1)$$

For Bi2212,  $T_{c,max} = 95$  K. The superconducting phase is approximately located between  $p = 0.05$  and  $0.27$ , having the maximum critical temperature  $T_{c,max}$  in the middle, thus at  $p \simeq 0.16$ . The corresponding phase-coherence energy scale  $\Delta_c$  is proportional to  $T_c$  as  $2\Delta_c = \Lambda k_B T_c$ , where  $k_B$  is the Boltzmann constant. In different

cuprates, the coefficient  $\Lambda$  is slightly different:  $\Lambda \simeq 5.4$  in Bi2212;  $\Lambda \simeq 5.1$  in YBCO; and  $\Lambda \simeq 5.9$  in  $Tl_2Ba_2CuO_6$  (Tl2201) [3].

In the literature, there are ample evidence for the existence of the so-called quantum critical point in cuprates (see references in [3]). In a quantum critical point located at/near absolute zero, the magnetic order is about to form or to disappear. In figure 2, the quantum critical point in Bi2212 exists at  $p \simeq 0.19$ . At low temperature, superconductivity in cuprates is most robust at this doping level  $p = 0.19$ , and not at  $p = 0.16$  (see below why).

In figure 2, the temperature scale  $T_{MT}$  starts/ends in the quantum critical point (MT = Magnetic Transition). Then, it is more or less obvious that this temperature/energy scale has a magnetic origin. The temperature scale  $T_{MT}$  is analogous with a magnetic transition temperature of long-range antiferromagnetic phase in heavy fermions [3]. The doping dependence  $T_{MT}(p)$  can be expressed as

$$T_{MT}(p) \simeq T_{MT,0} \times \left[1 - \frac{p}{0.19}\right], \quad (2)$$

where  $T_{MT,0} = 970\text{--}990$  K (see references in [3]). As was mentioned above, this energy scale is inferred from resistivity, nuclear magnetic resonance and specific heat measurements. Magnetic fluctuations are strong along the transition temperature  $T_{MT}(p)$ .

In figure 2, the energy scale with a characteristic temperature  $T_{CO}$  corresponds to a charge ordering (CO) in shape of quasi-one-dimensional stripes. A structural phase transition precedes the charge ordering. The doping dependence  $T_{CO}(p)$  can approximately be expressed as follows [3]

$$T_{CO}(p) \simeq 980 \times \left[1 - \frac{p}{0.3}\right] \quad (\text{Kelvins}). \quad (3)$$

The corresponding charge gap  $\Delta_{cg}$  observed in tunneling and ARPES spectra depends on hole concentration as

$$\Delta_{cg}(p) \simeq 251 \times \left[1 - \frac{p}{0.3}\right] \quad (\text{meV}). \quad (4)$$

In cuprates, manganites and nickelates, the charge ordering always precedes a magnetic ordering (MO) [3]. In figure 2, the energy scale with a characteristic temperature  $T_{MO}$  corresponds to an antiferromagnetic ordering occurring in insulating stripes which separate charge stripes. This magnetic ordering stabilizes the charge order which becomes long-ranged at  $T_{MO}$ . The doping dependence  $T_{MO}(p)$  can be expressed as follows

$$T_{MO}(p) \simeq 566 \times \left[1 - \frac{p}{0.3}\right] \quad (\text{Kelvins}). \quad (5)$$

The dynamical two-dimensional magnetic stripes can be considered as a local memory effect of the commensurate antiferromagnetic phase.

In figure 2, the temperature scale  $T_{pair}$  corresponds to the formation of Cooper pairs, the doping dependence of which can be expressed as

$$T_{pair}(p) \simeq \frac{T_{CO}(p)}{3} = \frac{980}{3} \times \left[1 - \frac{p}{0.3}\right] \quad (\text{Kelvins}). \quad (6)$$

The corresponding pairing energy scale  $\Delta_p$  depends on doping level as follows

$$\Delta_{pair}(p) \simeq \frac{\Delta_{cg}(p)}{3} = \frac{251}{3} \times \left[1 - \frac{p}{0.3}\right] \quad (\text{meV}). \quad (7)$$

The pairing gap manifests itself in tunneling and ARPES measurements. The extensions of three dependences  $T_{CO}(p)$ ,  $T_{MO}(p)$  and  $T_{pair}(p)$  cut the horizontal axis *approximately* in one point, at  $p = 0.3$ .

In figure 2, the spin-glass temperature scale  $T_g$  is shown schematically. For example, the temperature scale  $T_g$  in LSCO linearly increases as the doping starts to increase from zero, reaches its maximum when it crosses a Néel temperature scale  $T_N$ , and then decreases to zero as the doping increases. In Bi2212,  $T_g \simeq 8$  K at  $p = 0.05$ , and  $T_g = 0$  somewhere at  $p \simeq 0.15$  [4].

It is worth noting that, in first approximation in Bi2212, the two energy scales with characteristic temperatures  $T_{CO}$  and  $T_{MT}$  intersect the vertical axis in one point, at  $T \approx 980$  K. Some discussion on this issue can be found elsewhere [3].

It is necessary to mention that the above formula are approximate. To understand why, consider just one temperature/energy scale—the charge ordering scale  $T_{CO}$ . From acoustic measurements, it is well known that any structural phase transition has a hysteresis on lowering and on increasing the temperature. Since in cuprates, a structural phase transition precedes the charge ordering, its hysteresis may affect the charge ordering temperature scale. As a consequence, the above expression for  $T_{CO}(p)$  is most likely approximate. Secondly, the real doping dependences of temperature scales  $T_{MT}$ ,  $T_{CO}$ ,  $T_{MO}$  and  $T_{pair}$ , most likely, are not linear but quasi-linear.

#### IV. CHARGE INHOMOGENEITIES: PHASE SEPARATION

Let us go back to the question raised above: Why do different experimental techniques give different energy/temperature scales? As a matter of fact, this question is related to another question, namely, how is it possible that there are several magnetic temperature/energy scales in one phase diagram (see figure 2)?

Consider  $\text{CuO}_2$  planes at different doping levels. In undoped region ( $p < 0.05$ ), the doped holes gather into clusters having a size of a few nanometers. These clusters are embedded in an antiferromagnetic background where

the long-range antiferromagnetic order is preserved. In the clusters, the holes are not distributed homogeneously, but they form quasi-one-dimensional stripes along the diagonal direction relative to the Cu–O–Cu bonds [6]. In figure 3, this type of clusters is marked by B. The spin glass appears in these clusters at  $T_g$  [6].

In underdoped region, thus above  $p = 0.05$ , the charge stripes in most clusters are rotated by  $45^\circ$  relative to those in undoped region. Thus, they now run along the Cu–O–Cu bonds, and the distance between stripes becomes smaller than that between diagonal stripes. However, in a small fraction of clusters, the charge stripes remain diagonally oriented. This explains the existence of spin glass in the superconducting phase. The clusters with vertically (horizontally) oriented charge stripes are schematically shown in figure 3 by C. Thus, in deep underdoped region, the two types of clusters—with vertical stripe order and with diagonal stripe order—are embedded in an antiferromagnetic background. Therefore, the long-range antiferromagnetic phase which is usually located at low doping level extends to higher dopings. The doped holes are sucked out by the clusters. As a consequence, the Néel temperature scale  $T_N$  literally transforms into the temperature scale  $T_{MT}$  shown in figure 2. In a sense, the temperature scale  $T_{MT}$  is an echo of the  $T_N$  scale.

Near optimally doped region, the picture is different: now clusters with intact antiferromagnetic order are embedded in a charge-stripe background. In figure 3, the antiferromagnetic clusters are shown by A. At  $p = 0.19$ , this type of clusters completely vanishes, as schematically shown in figure 4(a). At the same time, the fraction of clusters with vertical charge stripes is maximal at  $p = 0.19$ , as shown in figure 4(b). Since superconductivity in cuprates occurs in these clusters, this is the reason why it is most robust at  $p = 0.19$ , and not at  $p = 0.16$ .

The three temperature scales,  $T_{MT}$ ,  $T_g$  and  $T_{MO}$  shown in figure 2, originate from a magnetic ordering in different clusters—A, B and C in figure 3, respectively. Since different experimental techniques are sensitive to different types of correlations, and have different resolutions and different characteristic times, it is then obvious why there is a discrepancy among phase diagrams presented in the literature.

Finally, let us consider the deep overdoped region. In deep overdoped region, new doped holes gather between stripes, forming clusters with Fermi sea, in which the hole distribution is more or less homogeneous. The Fermi-sea clusters, shown schematically in figure 3 by D, are embedded in a charge-stripe background. Since, the superconducting phase vanishes at  $p = 0.27$ , it is commonly assumed that above this doping level, the hole distribution becomes homogeneous in  $\text{CuO}_2$  planes. In fact, this assumption may be not true: The three temperature scales  $T_{CO}$ ,  $T_{MO}$  and  $T_{pair}$  in figure 2 originate from different types of ordering in clusters with vertical charge stripes.

Since these three temperature scales cut the horizontal axis approximately at  $p = 0.3$ , as shown in figure 2, it is possible that between  $p = 0.27$  and  $0.3$ , the hole distribution in  $\text{CuO}_2$  planes is not completely homogeneous. The clusters with vertical charge stripes may exist between  $p = 0.27$  and  $0.3$ , being embedded in a Fermi-sea background. In this case, the hole distribution in  $\text{CuO}_2$  planes is homogeneous only above  $p = 0.3$ , as schematically shown in figure 4(a). After all, this is not very important for understanding the mechanism of high- $T_c$  superconductivity.

## V. STRIPE PHASE

Since superconductivity in cuprates occurs in clusters with vertical charge stripes, it is most important to understand the physics of this phase. The size of clusters with vertical charge stripes depends on the doping level: In underdoped region, the size of these clusters is about  $30 \text{ \AA}$  [7]. Then, it is obvious that the length of charge stripes is of the same magnitude. In overdoped region, the length of charge stripes increases up to  $100 \text{ \AA}$  [8]. Therefore, the length of charge stripes also depends on the doping level.

Since charge stripes in cuprates are very dynamical, one may wonder how it is possible to observe charge-stripe domains by tunneling [7, 8]. First of all, there are two types of dynamics involved: the fluctuation of charge stripes inside clusters, and the clusters fluctuate as whole. Superconductivity most likely requires the former but not the latter. Secondly, the charge stripes can slow down in one separate cluster, this will not affect superconductivity locally **if** the charge stripes in the neighboring clusters go on fluctuating [3]. Generally speaking, the charge stripes can be pinned by an impurity, by a lattice defect, or by the surface.

It is commonly assumed that the charge-stripe orientation in adjacent  $\text{CuO}_2$  layers is alternately rotated by  $90^\circ$ . In fact, this assumption is not necessary: Depending on doping level, the clusters with *vertical* charge stripes may coexist in the same  $\text{CuO}_2$  layer with clusters having *horizontal* charge stripes [3].

## VI. SUMMARY

We discussed here a phase diagram of hole-doped cuprates and the origins of different temperature/energy scales. Hole-doped cuprates have a very rich phase diagram as a function of doping. This is due to a charge inhomogeneity in  $\text{CuO}_2$  planes: the charge distribution in  $\text{CuO}_2$  planes is inhomogeneous both on a nanoscale and macroscale. Depending on the doping level, the  $\text{CuO}_2$  planes comprise at least four different types of clusters

having a size of a few nanometers. Each type of clusters has its own features. As a consequence, the common phase diagram consists of, at least, seven different energy/temperature scales. As an example, we considered a phase diagram of  $\text{Bi}_2\text{Sr}_2\text{CaCu}_2\text{O}_{8+x}$ .

- 
- [1] Bednorz J G and Müller K A 1986 *Z. Phys. B* **64** 189
  - [2] Orenstein J and Millis A J 2000 *Science* **288** 468
  - [3] Mourachkine A 2002 *High-Temperature Superconductivity in Cuprates: The Nonlinear Mechanism and Tunneling Measurements*, (Dordrecht: Kluwer Academic)
  - [4] Panagopoulos C, Tallon J L, Rainford B D, Xiang T, Cooper J C and Scott C A 2002 *Phys. Rev. B* **66** 064501
  - [5] Presland M R, Tallon J L, Buckley R G, Lui L S and Flower N F 1991 *Physica C* **176** 95
  - [6] Matsuda M, Fujita M, Yamada K, Birgeneau R J, Endoh Y and Shirane G 2001 *preprint* cond-mat/0111228
  - [7] Lang K M, Madhavan V, Hoffman J E, Hudson E W, Eisaki Uchida S and Davis J C 2002 *Nature* **415** 412
  - [8] Howald C, Eisaki H, Kaneko N, Greven M and Kapitulnik A 2002 *preprint* cond-mat/0208442

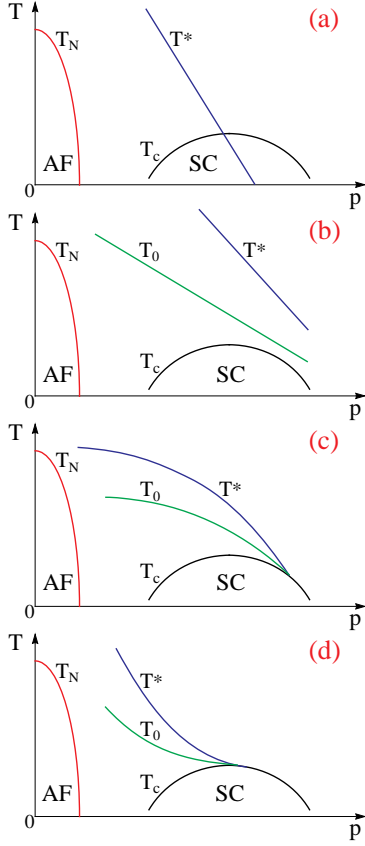


FIG. 1. Different phase diagrams of superconducting cuprates, which can be found in the literature.  $T_N$  is the Néel temperature;  $T_c$  is the critical temperature;  $T^*$  is the pseudogap temperature; and  $T_0$  is the pairing temperature (AF = antiferromagnetic; SC = superconducting).

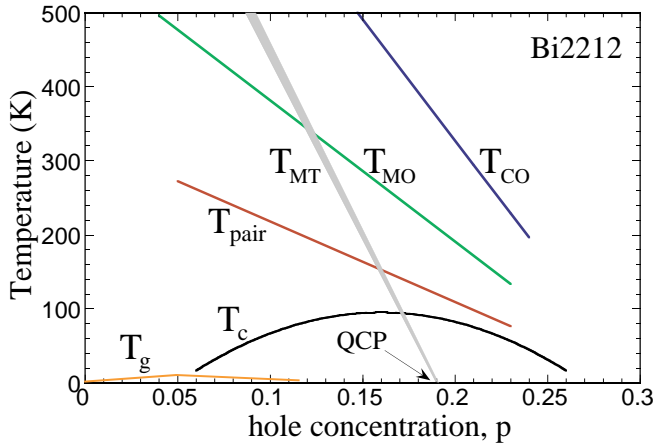


FIG. 2. Phase diagram of Bi2212 [3].  $T_c$  is the critical temperature;  $T_{pair}$  is the pairing temperature;  $T_{MT}$  is the magnetic-transition temperature;  $T_{MO}$  is the magnetic-ordering temperature; and  $T_{CO}$  is the charge-ordering temperature (for more details see text). The commensurate antiferromagnetic phase at low doping is not shown. The spin-glass temperature scale  $T_g$  is shown schematically (QCP = quantum critical point).

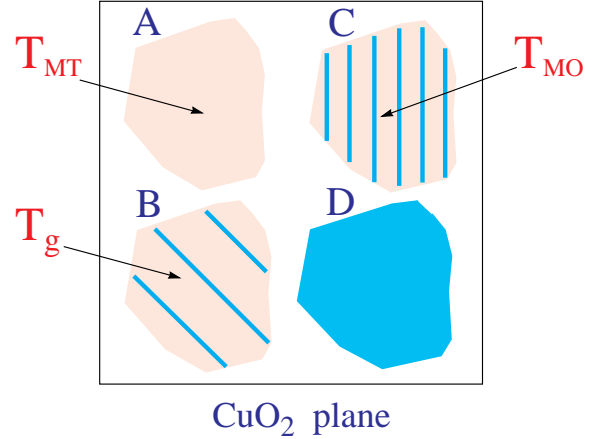


FIG. 3. Schematic representation of four types of clusters existing in  $\text{CuO}_2$  planes at different dopings. Cluster A includes a virgin antiferromagnetic phase. Cluster B includes diagonal charge stripes and a magnetic ordering between the stripes. The stripes are schematically shown by the lines. Cluster C includes vertical charge stripes and a magnetic ordering between the stripes. In cluster D, holes are distributed homogeneously (the Fermi sea). The magnetic ordering in clusters A, B and C occurs at  $T_{MT}$ ,  $T_g$  and  $T_{MO}$ , respectively.

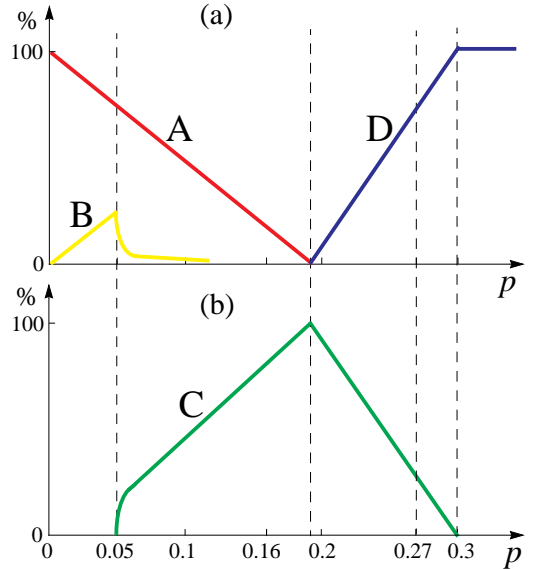


FIG. 4. (a) Fractions of clusters (phases) A, B and D in figure 3 in a  $\text{CuO}_2$  plane as a function of doping. (b) Fraction of clusters (phase) C. Both plots are shown schematically.